Supplementary Information (SI) for Journal of Materials Chemistry C.

Supporting Information

Theoretical design of homojunction solar cells based on chalcopyrite $AgInSe_2$: a combined study of first-principles calculations and device simulations

Jiancheng Zhong,[1] Changqing Lin,[1] Yang Xue,[1] Clas Persson,[2] and Dan Huang[1, 3, 4, *]

[1] Guangxi Novel Battery Materials Research Center of Engineering Technology, State Key Laboratory of Featured Metal Materials and Life-cycle Safety for Composite Structures, School of Physical Science and Technology, Guangxi University, Nanning 530004, China

[2] Department of Materials Science and Engineering, KTH Royal Institute of Technology, SE-100 44, Stockholm

[3] Guangxi Key Laboratory of Precision Navigation Technology and Application, Guilin University of Electronic Technology, Guilin 541004, China

[4] Guangxi Key Laboratory of Electrochemical Energy Materials, School of Chemistry and Chemical Engineering, Guangxi University, Nanning 530004, China

**danhuang@gxu.edu.cn*

S1. The $AgInSe_2$ crystal structures with different space groups

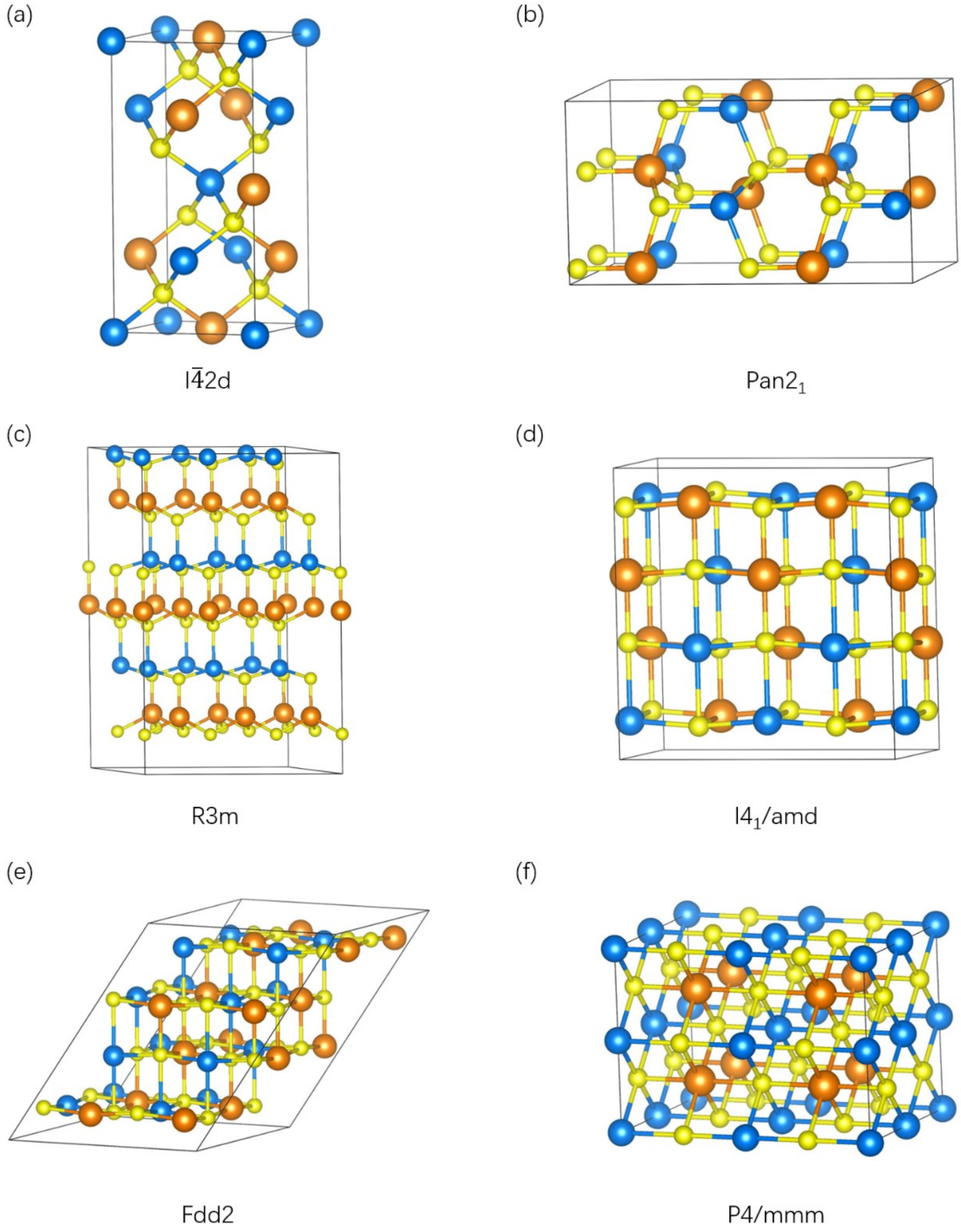

Figure S1. The crystal structures of $AgInSe_2$ are presented for different space groups: $I\bar{4}2d$ (a), $Pna2_1$ (b), R3m (c), $I4_1/amd$ (d), Fdd2 (e), and P4/mmm (f). Here, the blue, orange, and yellow spheres represent the Ag, In, and Se atoms, respectively.

.

We have calculated the total energies of $AgInSe_2$ structures in different space groups ($I\bar{4}2d$, Pna21, R3m, I41/amd, Fdd2, and P4/mmm) from the Materials Project crystal database,[1] as shown in Figure S1. The lattice constants and total energies of the structures with the six space groups are listed in Table S1. The calculation results show that the structure in the $I\bar{4}2d$ space group has the lowest total energy. In addition, $AgInSe_2$ with the $I\bar{4}2d$ space group has been widely reported in experiment.[2,3] Therefore, we adopt $AgInSe_2$ with the $I\bar{4}2d$ space group to carry out subsequent calculations on electronic structure, optical and defect properties, as well as device simulation studies.

Table S1. The calculated lattice constants and total energy differences (ΔE_{tot}) of $AgInSe_2$ in six space group. The total energy of $I\bar{4}2d$ is set as zero.

		Lattice constants		ΔE_{tot} (meV/f.u.)
Phase	*a* (Å)	*b* (Å)	*c* (Å)	
$I\bar{4}2d$	6.16	6.16	11.90	0
$Pna2_1$	7.06	7.06	8.66	0.04
R3m	2.16	2.16	21.01	1.59
$I4_1/amd$	5.65	5.65	11.41	2.24
Fdd2	5.65	5.65	5.71	2.23
P4/mmm	3.94	3.94	5.69	3.51

S2. Calculation details of defect formation energy

In this work, the used the following equation to calculate the defect formation energy[4-6]:

$$\Delta E(\alpha,q) = E(\alpha,q) - E(host) + \Sigma_i n_i(\Delta\mu_i + \mu_i) + q(E_v + E_F + \Delta V) + E_{corr},\#(S.1)$$

where $E(\alpha,q)$ is the total energy of the supercell with a defect α in the charge state q, while $E(host)$ is the corresponding energy for a defect-free system. Further, n_i is the number of atoms added into (n_i = –1) or removed from (n_i = +1) the supercell for the element i during the formation of the defect. $\Delta\mu_i$ is the relative chemical potential to correct the computed chemical potential μ_i of the elemental solid/gas. E_v is the valence band maximum (VBM) of the defect-free system, E_F is the Fermi level, referenced to the VBM, and ΔV is the potential correction between the perfect crystal and the defect system. In addition, we have accounted for the image charge correction term in our calculations. The image charge correction term is calculated by the following equation[7]:

$$E_{corr} = \frac{2}{3}n^2\frac{E_{wald}}{\varepsilon_0}.\#(S.2)$$

S3. Stability of $AgInSe_2$

Currently, there is no direct research on the stability of $AgInSe_2$ solar cells. Therefore, we derive relevant conclusions by investigating the more mature $CuInSe_2$, $MAPbI_3$, and $FAPbI_3$ systems. Analysis of the chemical potential regions of $AgInSe_2$, $CuInSe_2$, $MAPbI_3$, and $FAPbI_3$ via first-principles calculations indicates that the chemical potential region of $AgInSe_2$ is similar in size to that of $CuInSe_2$ and significantly larger than those of $MAPbI_3$ and $FAPbI_3$.[8-10] This implies that the stability of $AgInSe_2$ is comparable to that of $CuInSe_2$ and superior to those of $MAPbI_3$ and $FAPbI_3$. In addition, both $AgInSe_2$ and $CuInSe_2$ adopt a diamond-like structure, which is associated with notable thermodynamic and structural stability.[11,12] Given that $CuInSe_2$ solar cells have demonstrated reliable operational stability in long-term tests,[13,14] it is reasonable to infer that $AgInSe_2$ solar cells would exhibit comparable stability under practical conditions.

S4. Regulation of chemical potentials for $AgInSe_2$ preparation

We deeply appreciate your constructive suggestions, as the perspective you proposed has significantly enhanced the experimental guidance value of the manuscript. By integrating the mature experience from systems such as $Cu_2ZnSnSe_4$ (CZTSe) and $Cu(In,Ga)(S,Se)_2$ (CIGSSe), we elaborate on the experimental implementation mechanism of combining chemical potential control with annealing in $AgInSe_2$ from the perspective of synergistic regulation of preparation atmosphere and annealing process.

Chen et al.'s[15] computational investigations on CZTSe reveal that under Cu-poor and Zn-rich conditions ($Cu/(Zn+Sn)\approx0.8$, $Zn/Sn\approx1.2$), the concentration of the detrimental defect cluster $[2Cu_{Zn}+Sn_{Zn}]$ decreases significantly. Under such conditions, Cu vacancies (V_{Cu}) emerge as the dominant acceptor defects, capable of providing moderate hole concentrations while mitigating excessive carrier recombination. Li et al.[16] further validated this theoretical prediction experimentally: they first deposited a Cu/Zn/Sn metallic precursor by sputtering (controlling Cu/(Zn+Sn) = 0.70-0.75 and Zn/Sn = 1.10-1.15), followed by pre-alloying at 250 °C, soft selenization pretreatment at 280 °C, and finally annealing at 550 °C. This process promoted grain growth and improved the open - circuit voltage, increasing the photoelectric conversion efficiency (PCE) of CZTSe solar cells from 9.2% to 12.5%. This improvement validates that the combination of "precursor ratio + atmosphere + annealing" serves as an effective approach to integrate chemical potential control with annealing.

For the $AgInSe_2$ system, the research by Panda et al.[17] provides direct references for its preparation. They prepared n-type $AgInSe_2$ films by adjusting the Ag/In target ratio, confirming that regulating the target composition is a direct means of chemical potential control. Meanwhile, the initial phase was formed via selenization at 250 °C, followed by high-temperature annealing at 500 °C to promote the decomposition of impurity phases and element diffusion, ultimately optimizing the crystallinity and optoelectronic properties of n-$AgInSe_2$ films. Similarly, p-$AgInSe_2$ can be prepared by adjusting the target ratio.

In specific experimental operations, the chemical potential regulation of $AgInSe_2$ can be achieved through two core methods: first, adjusting the Ag/In ratio during sputtering to correspond to Ag-rich or Ag-poor growth points; second, regulating the Se partial pressure during the soft selenization stage to create a Se-rich environment. These methods can meet the chemical potential requirements for n-type (Point E: Ag-rich, In-poor, Se-rich) and p-type (Point C: Ag-poor, In-poor, Se-rich) materials. Meanwhile, the annealing temperature should be controlled at 600–800 K to promote crystallization and suppress the generation of harmful defects.

In summary, the experimental framework of "chemical potential regulation via atmosphere control and equilibrium promotion via annealing" in CZTSe, integrated with the specific methodologies of Panda et al. in $AgInSe_2$, establishes a comprehensive paradigm for combining chemical potential engineering with annealing processes. Additionally, Yang et al.[18] employed DC sputtering to form a Cu-deficient ordered vacancy compound layer in the CIGSSe system, creating a high-performance buried homojunction with CIGSSe to fabricate homojunction structures. This achievement validates the feasibility of preparing $AgInSe_2$ homojunction solar cells via sputtering.

S5 Interface states of $AgInSe_2$ homojunction solar cell

The key factor influencing interface states is the interfacial defect concentration, as it directly determines the strength of interfacial recombination. The interfacial defect concentration is positively correlated with the degree of lattice mismatch.[19,20] The advantage of homojunction solar cells over heterojunction solar cells lies in the lattice matching at the junction interface,[21,22] so interfacial recombination at the junction can be neglected. The interfacial defect concentration between n-$AgInSe_2$ and ITO can be studied using the ElectronLatticeMatch (ELM) code,[23] and the resulting lattice mismatch is listed in Table S2. The lattice mismatch between the (001) plane of $AgInSe_2$ and the (001) plane of ITO is only 0.49%, outperforming the 2.70% and 2.10% mismatches at the interfaces of Cu_2ZnSnS_4/CdS and Cu(In,Ga)Se_2/CdS, respectively.[4] Additionally, the lattice mismatch between the (100) plane of $AgInSe_2$ and the (110) plane of ITO is 3.35%, which is also within an acceptable range. This indicates that n-$AgInSe_2$ and ITO should exhibit low interface state density and low contact resistance.

Table S2. Lattice mismatch between the absorber and adjacent layers from the ELM screening.

absorber	adjacent layer	lattice mismatch (%)
$AgInSe_2$ (001)	ITO (001)	0.49
$AgInSe_2$ (100)	ITO (110)	3.35
Cu_2ZnSnS_4 (110)	CdS (110)	2.70
Cu(In,Ga)Se_2 (001)	CdS (001)	2.10

REFERENCES

(1) P. Qiu, Y. Qin, Q. Zhang, R. Li, J. Yang, Q. Song, Y. Tang, S. Bai, X. Shi and L. Chen, *Adv. Sci.*, 2018, **5**, 1700727.

(2) J. Su, Y. Liu, Y. Li, S. Bai, D. Gao, P. Chen, Z. Zhao, V. P. Dravid, H. Xie, L.-D. Zhao and M. G. Kanatzidis, *J. Am. Chem. Soc.*, 2025, **147**, 16611–16619.

(3) M. Kaleli, D. A. Aldemir and M. Parlak, *Appl. Phys. A*, 2017, **123**, 593.

(4) C. Lin, Y. Xue, C. Persson and D. Huang, *ACS Appl. Mater. Interfaces*, 2024, **16**, 52252–52263.

(5) Y. Huang, C. Lin, Y. Xue, B. Huang and D. Huang, *Phys. Chem. Chem. Phys.*, 2024, **26**, 28958–28970.

(6) J. Zhong, X. Zhang, C. Lin, Y. Xue, H. Tang, D. Huang, *Acta Phys. Sin.*, 2024, **73**, 103101.

(7) S. Lany and A. Zunger, *Phys. Rev. B*, 2008, **78**, 235104.

(8) N. Kim, P. P. Martin, A. A. Rockett and E. Ertekin, *Phys. Rev. B*, 2016, **93**, 165202.

(9) W. Ming, S. Chen and M.-H. Du, *J. Mater. Chem. A*, 2016, **4**, 16975–16981.

(10) N. Liu and C. Yam, *Phys. Chem. Chem. Phys.*, 2018, **20**, 6800–6804.

(11) D. R. Tallant, J. E. Parmeter, M. P. Siegal and R. L. Simpson, *Diam. Relat. Mater.*, 1995, **4**, 191–199.

(12) A. Grill, *Diam. Relat. Mater.*, 1999, **8**, 428–434.

(13) A. Rockett and R. W. Birkmire, *J. Appl. Phys.*, 1991, **70**, R81–R97.

(14) H. Azimi, Y. Hou and C. J. Brabec, *Energy Environ. Sci.*, 2014, **7**, 1829–1849.

(15) S. Chen, A. Walsh, X. Gong and S. Wei, *Adv. Mater.*, 2013, **25**, 1522–1539.

(16) J. Li, Y. Huang, J. Huang, G. Liang, Y. Zhang, G. Rey, F. Guo, Z. Su, H. Zhu, L. Cai, K. Sun, Y. Sun, F. Liu, S. Chen, X. Hao, Y. Mai and M.

A. Green, *Adv. Mater.*, 2020, **32**, 2005268.

(17) R. Panda, M. Panda, H. Rath, U. P. Singh, R. Naik and N. C. Mishra, *Opt. Mater.*, 2018, **84**, 618–624.

(18) J. Yang, J. Wang, Y. Gao, M. Chen, B. Chen, G. Zheng, D. Yao, N. Tian, P. Gan, H. Tan, P. Yang and F. Long, *Mat. Sci. Semicon. Proc.*, 2025, **195**, 109582.

(19) A. Moridi, H. Ruan, L. C. Zhang and M. Liu, *Int. J. Solids Struct.*, 2013, **50**, 3562–3569.

(20) Y. Wang, J. Li, Y. Zhou, Z. Gao, W. Zhu and L. Liu, *J. Alloys Compd.*, 2021, **872**, 159592.

(21) Y. Li, Z. Liu, J. Li, M. Ruan and Z. Guo, *J. Mater. Chem. A*, 2020, **8**, 6256–6267.

(22) N. Ali, R. Ahmed, J. T. Luo, M. Wang, A. Kalam, A. G. Al-Sehemi and Y. Q. Fu, *Mat. Sci. Semicon. Proc.,* 2020, **107**, 104810.

(23) K. T. Butler, Y. Kumagai, F. Oba and A. Walsh, *J. Mater. Chem. C*, 2016, **4**, 1149–1158.